

Leptonic decays of the Σ^- and Ξ^- hyperons

W. Tanenbaum,* V. Hungerbühler,† R. Majka, J. N. Marx, P. Némethy, J. Sandweiss, and W. J. Willis‡
Yale University, New Haven, Connecticut 06520§

M. Atac, S. Ecklund, P. J. Gollon, J. Lach, J. MacLachlan, A. Roberts, R. Stefanski, and D. Theriot
Fermi National Accelerator Laboratory, Batavia, Illinois 60510||

C. L. Wang

Brookhaven National Laboratory, Upton, New York 11973¶

(Received 24 February 1975)

The decays $\Sigma^- \rightarrow ne^- \bar{\nu}$, $\Sigma^- \rightarrow \Lambda e^- \bar{\nu}$ ($\Lambda \rightarrow \pi^- p$), and $\Xi^- \rightarrow \Lambda e^- \bar{\nu}$ ($\Lambda \rightarrow \pi^- p$) were studied using unpolarized hyperons from the Yale-Fermilab-BNL hyperon beam at the Brookhaven National Laboratory Alternating Gradient Synchrotron. The Σ^- , Ξ^- , e^- , and Λ -decay-product momenta were measured by magnetic spectrometers with magnetostrictive wire spark chambers. A threshold Čerenkov counter and a total absorption calorimeter identified the electron and neutron, respectively. From a sample of 3507 reconstructed $\Sigma^- \rightarrow ne^- \bar{\nu}$ events we have found $|g_A/g_V| = 0.435 \pm 0.035$. From a sample of 55 reconstructed $\Sigma^- \rightarrow \Lambda e^- \bar{\nu}$ events we have found $g_V/g_A = -0.17 \pm 0.35$ assuming that the conserved vector current hypothesis correctly predicts the weak magnetic form factor. A new one-angle Cabibbo fit gives $f = 0.436 \pm 0.010$, $d = 0.812 \pm 0.011$, and $\theta = 0.232 \pm 0.003$ radian.

1. INTRODUCTION

Recently there has been great interest in the leptonic decays of hyperons as a test of the SU(3) structure of the weak hadronic currents. Assuming (i) a current-current interaction, (ii) that the leptonic current is the same as in the nuclear β decay (implying that only vector and axial-vector components exist in the hadronic current), and (iii) that the interaction is invariant under time reversal, the decay amplitude for $A \rightarrow Be\nu$, where A and B are spin- $\frac{1}{2}$ baryons, can be written as¹

$$M = \frac{G}{\sqrt{2}} \bar{u}_B \left(g_V \gamma_\mu + \frac{g_{WM}}{m_A} \sigma_{\mu\nu} q^\nu + \frac{g_S}{m_A} q_\mu + g_A \gamma_\mu \gamma^5 + \frac{g_{PT}}{m_A} \sigma_{\mu\nu} q^\nu \gamma^5 + \frac{g_P}{m_A} q_\mu \gamma^5 \right) u_A \times \bar{u}_e \gamma^\mu (1 - \gamma^5) u_\nu. \quad (1)$$

The six dimensionless form factors g are real scalar functions of q^2 , the square of the four-momentum transfer $q^\mu = p_A^\mu - p_B^\mu$.

For all baryon leptonic decays where both the initial and final baryons are members of the $\frac{1}{2}^+$ SU(3) octet, the dominant form factors g_V (vector) and g_A (axial vector) are predicted (at $q^2 = 0$) by the Cabibbo theory² in terms of three arbitrary parameters. Previous to this work, many hyperon β -decay experiments have been performed,³⁻⁶ but the validity of the Cabibbo theory was still in doubt. Except for $\Lambda \rightarrow pe^- \bar{\nu}$,⁷ measurements of g_A/g_V in hyperon leptonic decays still suffered from poor statistics. A high-statistics measurement of g_A/g_V , or even $|g_A/g_V|$, in the decay $\Sigma^- \rightarrow ne^- \bar{\nu}$ would have done much to clarify the situation.

The decays $\Sigma^\pm \rightarrow \Lambda e^\pm \nu$ are unique among hyperon leptonic decays in that the conserved-vector-current hypothesis (CVC) predicts that $g_V(q^2 = 0)$ is

zero.⁸ Measurement of g_V/g_A in $\Sigma^- \rightarrow \Lambda e^- \bar{\nu}$ thus provides a test of CVC. Reconstruction of $\Xi^- \rightarrow \Lambda e^- \bar{\nu}$ events would be an interesting technical achievement because no previous non-bubble-chamber experiment has been able to reconstruct complete events.

The four form factors g_{WM} , g_S , g_{PT} , and g_P are the so-called "small form factors" induced by the strong interactions. When the matrix element is evaluated, the g_S and g_P terms are proportional to m_e/m_A , which makes their contribution negligible in β decay. If B and A are in the same SU(3) multiplet, then g_{PT} vanishes only in the limit of SU(3) symmetry. If B and A are in the same isospin multiplet, charge symmetry requires that the form factor g_{PT} vanish.⁹ In the analysis of our experiments we always assumed $g_{PT} = 0$.

The form factor g_{WM} (weak magnetism) is predicted by CVC for all baryon leptonic decays with in the $\frac{1}{2}^+$ octet. The effects of the weak-magnet-

ism term on most experimental distributions of interest is small compared to that of the dominant form factors g_V and g_A .

In all three decays, $\Sigma^- \rightarrow ne^- \bar{\nu}$, $\Sigma^- \rightarrow \Lambda e^- \bar{\nu}$, and $\Xi^- \rightarrow \Lambda e^- \bar{\nu}$, the three-body final state can be completely kinematically analyzed. In the decay $\Sigma^- \rightarrow ne^- \bar{\nu}$, if we can observe the final neutron direction, we can reconstruct the decay to within a zero-constraint twofold ambiguity. In the other decays, we can reconstruct the $\Lambda \rightarrow p \pi^-$ decay, and thus the leptonic decay is once overconstrained. In addition, the Λ decay is a good analyzer of the Λ polarization (S_Λ), thus allowing us to measure the correlation between momenta and the Λ spin.

There are essentially five independent experimental distributions sensitive to the form factors. Let us first define three orthonormal vectors,³

$$\begin{aligned}\hat{\alpha} &= (\vec{p}_e + \vec{p}_\nu) / |\vec{p}_e + \vec{p}_\nu|, \\ \hat{\beta} &= (\vec{p}_e - \vec{p}_\nu) / |\vec{p}_e - \vec{p}_\nu|, \\ \hat{\gamma} &= (\vec{p}_e \times \vec{p}_\nu) / |\vec{p}_e \times \vec{p}_\nu|,\end{aligned}\quad (2)$$

and also the ratio

$$Z = g_V / g_A. \quad (3)$$

The following distributions are then of interest:

1. The center-of-mass baryon energy spectrum (or equivalently, the $e-\nu$ angular correlation) is highly sensitive to $|g_A/g_V|$.

2. The center-of-mass lepton energy spectrum which is weakly dependent on $[g_V + (1 + m_B/m_A)g_{WM}]g_A$. Thus, in principle at least, if g_{WM} is known, g_A/g_V (including its sign) can be determined even without polarization measurements. This dependence is first order in the momentum transfer q . For $\Sigma^- \rightarrow \Lambda e^- \bar{\nu}$, because of the small value of q^2 and our poor statistics, the effect is too small to be seen in our data. For $\Sigma^- \rightarrow ne^- \bar{\nu}$, we have sufficient statistical power to see this effect, and in the absence of polarized Σ^- this effect provides the only possibility of determining the sign of g_A/g_V . However, systematic biases in the electron detection make such a determination unreliable.

3. The $\hat{S}_\Lambda \cdot \hat{\alpha}$ spin correlation, which is sensitive to $\text{Re}Z$.

4. The $\hat{S}_\Lambda \cdot \hat{\beta}$ correlation, which is somewhat sensitive to $|Z|$.

5. The $\hat{S}_\Lambda \cdot \hat{\gamma}$ correlation, which is sensitive to $\text{Im}Z$. Our assumption of T invariance implies that this correlation vanishes.

Four of the expected distributions are given below in the approximation that the electron has zero mass and that the decay baryon is nonrelativistic³:

$$\begin{aligned}W(\cos\theta_{e\nu}) &= \frac{1}{2} \left(1 + \frac{|Z|^2 - 1}{|Z|^2 + 3} \cos\theta_{e\nu} \right), \\ W(\hat{S}_\Lambda \cdot \hat{\alpha}) &= \frac{1}{2} \left(1 + \frac{8}{3} \frac{\text{Re}Z}{|Z|^2 + 3} \hat{S}_\Lambda \cdot \hat{\alpha} \right), \\ W(\hat{S}_\Lambda \cdot \hat{\beta}) &= \frac{1}{2} \left(1 + \frac{8}{3} \frac{1}{|Z|^2 + 3} \hat{S}_\Lambda \cdot \hat{\beta} \right), \\ W(\hat{S}_\Lambda \cdot \hat{\gamma}) &= \frac{1}{2} \left(1 + \frac{\pi}{2} \frac{\text{Im}Z}{|Z|^2 + 3} \hat{S}_\Lambda \cdot \hat{\gamma} \right).\end{aligned}\quad (4)$$

All experiments are analyzed neglecting the q^2 dependence of all form factors. In $\Sigma^- \rightarrow \Lambda e^- \bar{\nu}$, this assumption is justified due to extremely small q^2 and poor statistics. In $\Sigma^- \rightarrow ne^- \bar{\nu}$, the introduction of a linear slope to the form factors g_A and g_V would introduce too many free parameters for a meaningful fit to be achieved.

II. APPARATUS

A beam of unpolarized Σ^- and Ξ^- was produced using the Yale-Fermilab-BNL high-energy negative-hyperon beam at the Brookhaven National Laboratory (BNL) Alternating Gradient Synchrotron (AGS).¹⁰ The hyperon beam delivers Σ^- and Ξ^- produced in the forward direction at a central momentum of 23 GeV/c. For a machine pulse of 1.5×10^{11} interacting protons, the flux¹¹ at the exit of the magnetic channel is approximately 200 Σ^- and 2 Ξ^- . Figure 1 depicts the beam and the associated electronic detection apparatus, which are described in more detail elsewhere.¹⁰ Beam particles of mass less than 1 GeV/c² are vetoed by a threshold Čerenkov counter (\check{C}_B) which forms part of the beam channel. This tagging scheme is reinforced by a scintillation counter (V_π) located at the downstream end of the apparatus whose function is to veto stable beam particles. A set of small counters (B) and a hole veto counter (V_H) define the beam and discriminate against upstream hyperon decays. A cluster of high-pressure high-resolution magnetostrictive spark chambers¹² determines the momentum of the emerging hyperons to $\pm 1\%$.

Located downstream of the 2.9-m decay region is a magnetic spectrometer with conventional magnetostrictive wire spark chambers, which determines the momentum of decay electrons or negative pions to about $\pm 5\%$. Situated after the spectrometer is a Čerenkov counter (\check{C}) filled with hydrogen at atmospheric pressure. This counter, which has a large phase-space acceptance, identifies electrons from the desired leptonic decay from among the more copious pions produced in the major decay modes, $\Sigma^- \rightarrow n \pi^-$ and $\Xi^- \rightarrow \Lambda \pi^-$. The

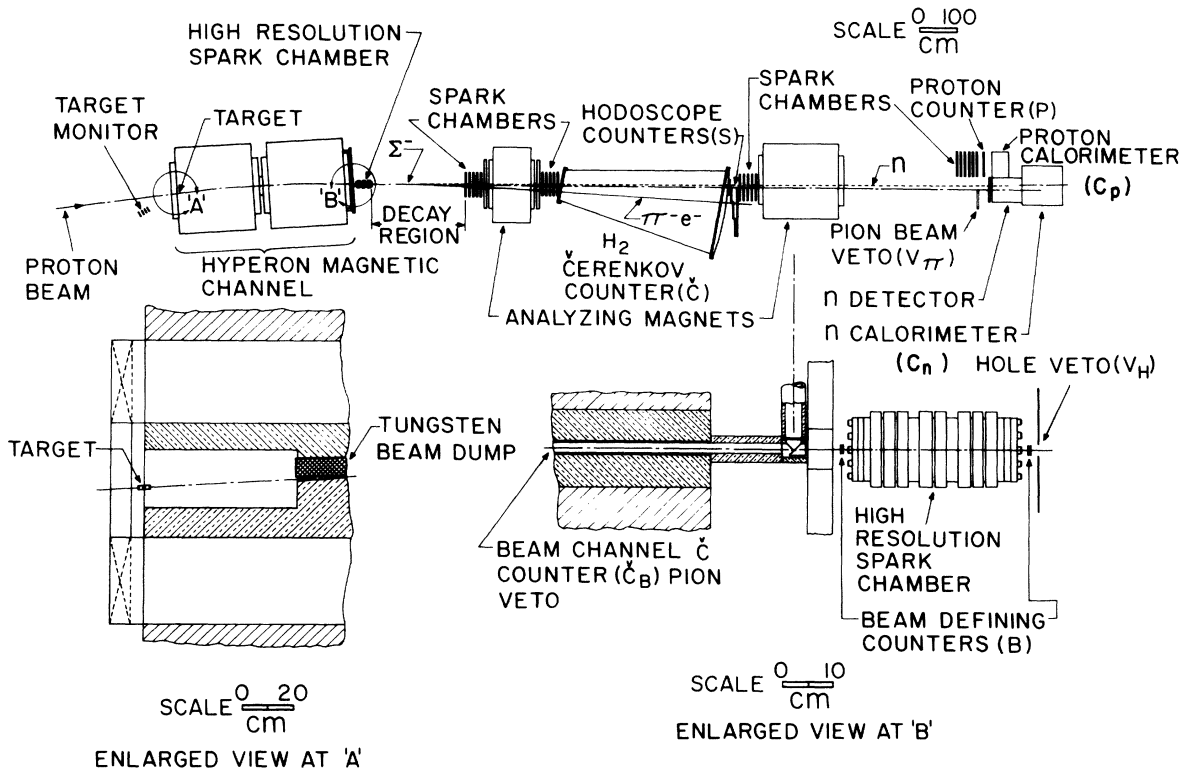


FIG. 1. Schematic diagram of the high-energy hyperon beam at the BNL AGS.

counter suppresses the trigger rate for the major decay modes by a factor of approximately 80. Following the Čerenkov counter is a hodoscope of scintillation counters (S), each of which shadows one of the five optical cells of the electron Čerenkov counter. In addition, the counter nearest to the beam line is backed by a lead and scintillator shower counter to give extra discrimination against nonleptonic backgrounds. A second spectrometer, located downstream of the Čerenkov counter, determines the momentum of the proton from the Λ decay to $\pm 5\%$. An iron-scintillator calorimeter (proton calorimeter, C_p) is the last component of the second spectrometer.

A neutron detector¹³ is also located at the downstream end of the apparatus on the neutral-beam line. It consists of a set of five modules, each having a 3.2-cm iron plate, an XY multiwire proportional chamber with 1-cm wire spacing, and a scintillation counter. It is followed by a second iron-scintillator hadron calorimeter (neutron calorimeter, C_n). The interaction point of the decay neutron is determined from the spatial distribution of the resulting hadron shower in the five

modules. By use of a complex algorithm¹⁴ the neutron interaction point can be determined to better than 1 cm (rms) for 80% of the events. As a result, the direction of the decay neutron is determined to better than 1 mrad.

The decay $\Sigma^- \rightarrow ne^- \bar{\nu}$ was signaled by the trigger $\bar{C}_B \cdot B \cdot \bar{V}_H \cdot \bar{C} \cdot S \cdot C_n \cdot \bar{V}_\pi$ (see Fig. 1). This trigger selects events with a massive beam particle, a low-momentum electron following the first spectrometer magnet and a fast neutron following the second spectrometer magnet. The neutron calorimeter was used to discriminate against background muons by requiring a minimum pulse height in the trigger. The crude information on the neutron energy ($\pm 25\%$) was not used in the reconstruction. Two-body decays, $\Sigma^- \rightarrow n\pi^-$, and beam pions were also recorded at a scaled-down rate to provide a flux normalization and to monitor the efficiency and resolution of the chambers and neutron detector. The total trigger rate was a few per machine pulse.

The decays $\Sigma^- \rightarrow \Lambda e^- \bar{\nu}$ and $\Xi^- \rightarrow \Lambda e^- \bar{\nu}$, followed by $\Lambda \rightarrow p\pi^-$, were signaled by the trigger $\bar{C}_B \cdot B \cdot \bar{V}_H \cdot \bar{C} \cdot S \cdot C_p \cdot \bar{V}_\pi$. Two-body decays, Ξ^-

$\rightarrow \Lambda\pi^-$, were also recorded at a scaled-down rate. A minimum pulse height in the proton calorimeter was required in the trigger to discriminate against background muons. For each trigger we recorded the configuration of scintillation-counter hits, the pulse heights from the electron Čerenkov counter, shower counter, neutron calorimeter, and proton calorimeter, the time difference between signals from the electron Čerenkov counter and the S counter hodoscope, as well as the spark chamber and multiwire proportional-chamber information. The major background in the leptonic triggers was a result of the decays $\Sigma^- \rightarrow n\pi^-$ and $\Xi^- \rightarrow \Lambda\pi^-$ in time with a background muon which triggered the electron Čerenkov counter. A major task of the analysis was to remove this background, which is three ($\Sigma^- \rightarrow n\pi^-$) or four ($\Xi^- \rightarrow \Lambda\pi^-$) times overconstrained, from the signal of leptonic decays. The muon background is discussed more fully in Appendix II.

III. $\Sigma^- \rightarrow ne^-\bar{\nu}$ ANALYSIS¹⁵

About one million $\Sigma^- \rightarrow ne^-\bar{\nu}$ triggers were recorded. Figure 2 indicates stages in the reduction of these triggers to 3507 accepted events.

A. Preliminary geometric cuts

The $\Sigma^- \rightarrow ne^-\bar{\nu}$ triggers were first required to meet the following requirements:

1. A beam track was required which could be extrapolated to the hyperon production target within the beam channel phase space.
2. The distance of closest approach between the beam track and the negative-decay-product track was required to be less than 6 mm in order to ensure a good decay vertex.
3. The kink angle between the beam track and the negative-decay-product track was required to be greater than 9 mrad. This ensured that the decay point could be reconstructed with adequate resolution.
4. The intersection of the beam track and the negative track was required to be within the 2.9-m decay fiducial region.

Most of the rejected triggers were Σ^- which decayed upstream of the decay region.

B. Neutron detection

The interaction point of the neutron in the neutron detector was then determined by a complex algorithm, which is described elsewhere.¹⁴ Approximately 20% of the event candidates were rejected because the algorithm failed to find a solution. The loss of candidates was found to be in-

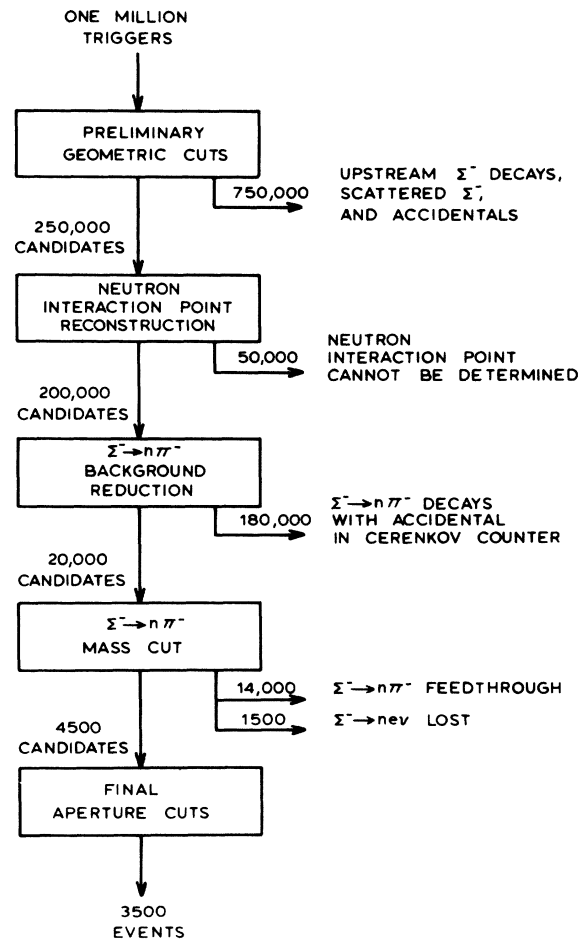


FIG. 2. Block diagram of $\Sigma^- \rightarrow ne^-\bar{\nu}$ data analysis.

dependent of the kinematics of the neutron in the Σ^- rest frame and so does not bias the results.

C. $\Sigma^- \rightarrow n\pi^-$ background rejection

Figure 3(a) shows the beam mass spectrum of leptonic candidates surviving the preliminary geometric cuts, reconstructed under the $\Sigma^- \rightarrow n\pi^-$ hypothesis. A 1-C reconstruction ignoring the neutron-detector information was used. The broad distribution contains the leptonic events, and the sharp peak at the Σ^- mass contains the two-body background. A reduction of the nonleptonic background was made by requiring a large pulse height in the shower counter when relevant, a tight timing correlation between the electron Čerenkov counter and appropriate S counter, and

by requiring that the reconstructed negative track point to the cell of the Čerenkov counter and the S counter that gave a pulse. These consistency requirements serve to further define decay electrons and eliminate events having an accidental background muon triggering the electron Čerenkov counter. The nonleptonic backgrounds are thus reduced to the level depicted in Fig. 3(b). The smooth curve in Fig. 3(b) indicates the excellent agreement between the data and the spectrum as generated by a Monte Carlo calculation (see Appendix I). The final sample of 3507 $\Sigma^- \rightarrow ne^- \bar{\nu}$ decays results from a cut requiring the reconstructed Σ^- mass, assuming the hypothesis $\Sigma^- \rightarrow n\pi^-$, to be less than 1165 MeV, and from the final aperture cuts described below.

D. Final aperture cuts

A detailed study of the distribution of electron impact points in the Čerenkov counter mirrors indicated that there were areas of relatively poor detection efficiency in the corners of the mirrors.¹⁵ Hence all electrons were required to intersect areas of better than 90% efficiency. Also, aperture cuts were imposed at all magnet apertures and for all scintillation counters that were required in the trigger.

IV. $\Sigma^- \rightarrow ne^- \bar{\nu}$ RESULTS

For this leptonic decay there is a square-root ambiguity resulting from the zero-constraint fit, so that we cannot assign an event to a unique position on a Dalitz plot. In order to obtain the maximum information in a bias-free manner, both solutions were kept and each event plotted on a two-dimensional plot. The smaller neutron energy and the larger neutron energy define the coordinates. The form-factor ratios were obtained from the final-event sample by a maximum-likelihood fit to this plot weighted by a Monte Carlo calculation of the acceptance of the detection apparatus. Our center-of-mass neutron resolution (about 5 MeV) corresponds to $\frac{1}{5}$ of the maximum possible neutron energy for each solution.

Data were taken for two values (6 kG m and 13 kG m) of the magnetic field in the spectrometer magnet. This had the advantage of giving two data samples with different amounts of nonleptonic backgrounds and different detection efficiencies. Figure 4 shows the binned two-dimensional neutron spectrum for the 6-kG m data. The results for the absolute value of the form-factor ratio as computed from a likelihood function (\mathcal{L}) fitted to the neutron spectra are presented in Table I. In obtaining these results, it was assumed that second-class currents are negligible and that the effect of

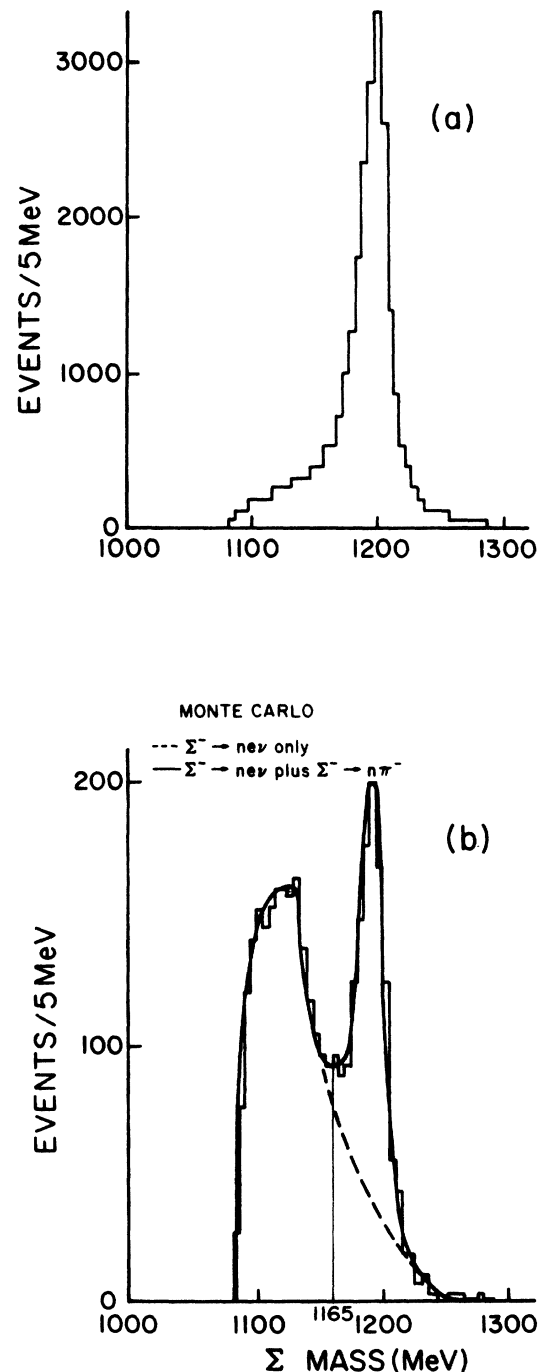


FIG. 3. (a) Mass spectrum of beam particles for leptonic decays at an early stage of the analysis when reconstructed under the $\Sigma^- \rightarrow n\pi^-$ hypothesis. The leptonic events being sought are in the broad tail; the two-body background events are in the sharp peak. (b) The same spectrum at the last stage in the analysis. The smooth curves indicate the shapes predicted by the Monte Carlo. A final mass cut of 1165 MeV was made and events below that mass were considered to be leptonic decays.

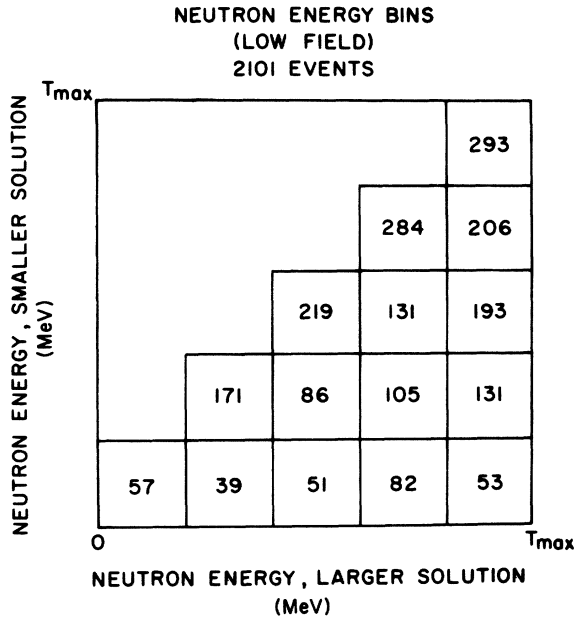


FIG. 4. Binned neutron center-of-mass energy spectrum for the 6-kG m data.

weak magnetism is that predicted by the CVC hypothesis. The result is quite insensitive to the amount of weak magnetism present. The full two-dimensional neutron spectra were used in the actual maximum-likelihood fit. We can also construct a one-dimensional spectrum by giving both solutions for the neutron energy equal weight. Figure 5 shows the resulting neutron spectrum for the 6-kG m data compared with expected spectra for $|g_A/g_V|=0.3$ and $|g_A/g_V|=0.5$. We present this comparison only to give a visual indication of the sensitivity of the measurement.

In order to evaluate the quality of the likelihood fit of the data to the usual parameterization of the weakly interacting hadronic current,¹ Monte Carlo

TABLE I. Results for $|g_A/g_V|$ and maximum-likelihood fits from neutron spectrum in c.m. system.

Spectrometer field integral	6 kG m	13 kG m
$ g_A/g_V $	0.420 ± 0.045	0.455 ± 0.055
$\ln \mathcal{L}(\text{data})$	-51.68	-52.11
$\ln \mathcal{L}(\text{Monte Carlo})$	-53.28 ± 3.26	-49.62 ± 3.18
Probability $\mathcal{L}(\text{Monte Carlo}) < \mathcal{L}(\text{data})$	69%	22%
Average of two field values	0.435 ± 0.035	

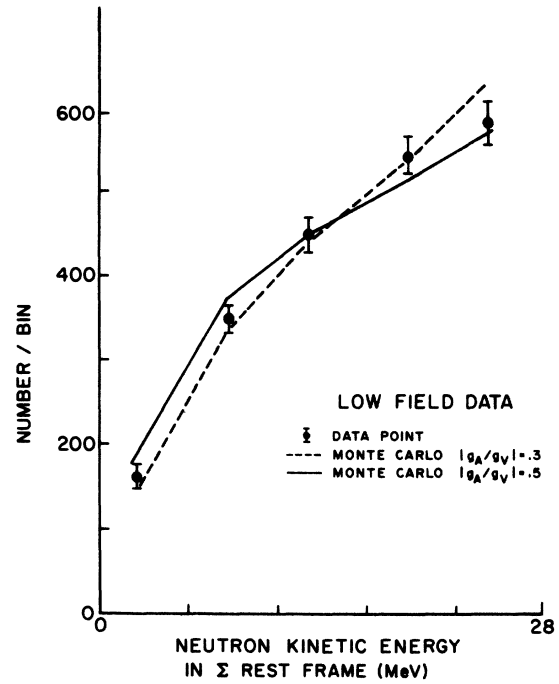


FIG. 5. A comparison of the experimentally determined neutron center-of-mass energy spectrum and those expected for two values of $|g_A/g_V|$. Both solutions for the neutron energy are used with equal weight. Data are for 6 kG m.

techniques were used to generate a number of event samples of equivalent statistical power to the data sample. The measured form-factor ratios were used as inputs to the Monte Carlo program (see Appendix I), which included the effects of experimental resolution. These events were then analyzed in a manner identical to that used for the data. Since the Monte Carlo generates events from the matrix element described in Ref. 1 with the measured value of $|g_A/g_V|$, the values of the likelihood function obtained for the Monte Carlo data samples represent those of a good fit to the input theory. The range of these likelihood values indicates the level of fluctuations due to the limited statistics (which matches that of the real data). A comparison between the value of the likelihood fits for the data and Monte Carlo generated event samples is presented in Table I. This comparison indicates a good probability that the data and Monte Carlo generated events sample the same parent populations. Thus, the value of the likelihood fit to the data indicates that the matrix element from Ref. 1 with the measured value of $|g_A/g_V|$ is the appropriate theoretical framework for understanding the data.

The detection efficiency calculated by the Monte

Carlo for the leptonic decays was 11% for the lower magnetic field and 10% for the higher field. Most of the loss was due to Σ^- decaying upstream of the fiducial region or to decay electrons hitting the spectrometer magnet. The probability of a decay electron hitting the spectrometer magnet or an inefficient region of the Čerenkov counter was extremely weakly correlated with the neutron center-of-mass energy. The size of the neutron detector was chosen to intercept all of the decay neutrons. The neutron detection efficiency was independent of angle and only weakly dependent on laboratory momentum (less than $\pm 5\%$ variation). Thus the detection efficiency was almost entirely independent of the neutron center-of-mass energy. The errors assigned to $|g_A/g_V|$ are purely statistical. None of the small systematic corrections considered contributes significant uncertainties. The $\Sigma^- \rightarrow n\pi^-$ background contamination after the mass cut was 1.5% (7.9%) of the leptonic sample for the 6-kGm (13-kGm) data as determined from the shape of the reconstructed mass spectrum of real $\Sigma^- \rightarrow n\pi^-$ events. This background was included in the Monte Carlo simulation. The result for $|g_A/g_V|$ was found to be insensitive to such background of up to 10%, even when such background was not included in the Monte Carlo. The final result for the absolute value of the form-factor ratio is obtained by taking a weighted average of the results from the two data samples to yield

$$|g_A/g_V| = 0.435 \pm 0.035.$$

Table II contains a comparison of this experiment with the results of previous experiments.

Our determination of $|g_A/g_V|$ has been made assuming that the form factors are independent of q^2 . We can calculate the effect that a linear q^2 dependence of the form factors would have on our result. Our result is fairly insensitive to a linear q^2 dependence of g_V , simply because at large q^2 (low neutron energy) the contribution of the vector interaction is small. However, the contribution of the axial-vector interaction is greatest at large q^2 , so that a q^2 dependence of g_A affects our result.

Let us assume

$$g_A(q^2) = g_A(0)(1 + \lambda_A q^2/m_\Sigma^2), \quad (5)$$

where λ_A is a dimensionless constant. Defining G_M as the measured value of $|g_A/g_V|$ assuming $\lambda_A = 0$ and G_0 as the value of $|g_A/g_V|$ at $q^2 = 0$, it can be shown¹⁵ that the approximate first-order effect of λ_A on our result is

$$G_M = G_0[(1 + \lambda'_A)/(1 - G_0^2 \lambda'_A)]^{1/2}, \quad (6)$$

where

$$\begin{aligned} \lambda'_A &= [2(m_\Sigma - m_n)^2/m_\Sigma^2] \lambda_A \\ &= 0.092 \lambda_A. \end{aligned} \quad (7)$$

Inverting, we get

$$G_0 = G_M \{1 + [2(m_\Sigma - m_n)^2/m_\Sigma^2] \lambda_A (1 + G_M^2)\}^{-1/2}, \quad (8)$$

or

$$\left| \frac{g_A}{g_V} \right|_{q^2=0} = G_M (1 + 0.110 \lambda_A)^{-1/2}. \quad (9)$$

From CVC, we take $\lambda_V \approx 2m_\Sigma^2/m_n^2 = +3.1$.¹⁶⁻¹⁸ Assuming $\lambda_A = \frac{1}{2} \lambda_V = +1.55$,¹⁹ we have $|g_A/g_V|_{q^2=0} = 0.924 G_M$. Thus, assuming $\lambda_A = +1.55$, our result becomes $|g_A/g_V|_{q^2=0} = 0.402 \pm 0.035$, where we have assumed that the statistical error is unaffected.

Our determination has also been made assuming the absence of second-class currents. The presence of an induced pseudotensor interaction affects our result primarily through the interference term between the induced pseudotensor interaction and the axial-vector interaction. Redefining G_m as the measured value of $|g_A/g_V|$ assuming $g_{PT} = 0$, it can be shown that the effect of this term on our result is

$$G_m = \left| \frac{g_A}{g_V} \right| \left(\frac{1 - g'_{PT}/g_A}{1 + |g_A/g_V|^2 (g'_{PT}/g_A)} \right)^{1/2}, \quad (10)$$

where

$$g'_{PT} = [2(m_\Sigma - m_n)/m_\Sigma] g_{PT} = 0.439 g_{PT}. \quad (11)$$

Inverting, we get

$$\left| \frac{g_A}{g_V} \right| = G_m [1 - (g'_{PT}/g_A)(1 + G_m^2)]^{-1/2}, \quad (12)$$

or

$$\left| \frac{g_A}{g_V} \right| = (0.435 \pm 0.035)(1 - 0.51 g_{PT}/g_A)^{-1/2}. \quad (13)$$

TABLE II. Summary of $\Sigma^- \rightarrow ne^{-}\bar{\nu}$ form-factor experiments.

Experiment	Year	No. of events	$ g_A/g_V $
Maryland ⁴	1969	49	0.23 ± 0.16
Heidelberg ⁵	1969	33	$0.37^{+0.26}_{-0.19}$
Columbia-Stony Brook ⁶	1972	36	$0.29^{+0.28}_{-0.29}$
This experiment	1975	3507	0.435 ± 0.035
New world average			0.413 ± 0.033

V. $\Sigma^- \rightarrow \Lambda e^- \bar{\nu}$ ANALYSIS

The same geometric cuts, pulse-height cuts, and Čerenkov-counter consistency requirements (except the 9-mrad decay-angle cut) used for $\Sigma^- \rightarrow ne^- \bar{\nu}$ were all used for $\Sigma^- \rightarrow \Lambda e^- \bar{\nu}$ triggers. The following additional requirements were imposed:

1. The distance of closest approach between the proton and π^- tracks must be less than 6 mm to ensure a good Λ vertex.
2. The Λ effective mass squared reconstructed from the π^- and proton tracks must have a value between 1.22 and 1.27 $(\text{GeV}/c^2)^2$.
3. The extrapolated reconstructed Λ^0 momentum vector must pass within 2 cm of the beam track decay vertex.

In addition, the momentum of the electron in the Σ^- rest frame was required to be less than 80 MeV/c. This last cut eliminates most of the remaining $\Xi^- \rightarrow \Lambda \pi^-$ background while eliminating no real $\Sigma^- \rightarrow \Lambda e^- \bar{\nu}$ events.

Fifty-five good reconstructed events were obtained, 34 at 6 kG m, and 21 at 13 kG m. The separation of $\Sigma^- \rightarrow \Lambda e^- \bar{\nu}$ from Ξ^- decays was very clean owing to the much smaller Q value of $\Sigma^- \rightarrow \Lambda e^- \bar{\nu}$. The expected level of $\Xi^- \rightarrow \Lambda \pi^-$ background in the final sample was three events.

An over-all simultaneous six-constraint fit was performed on the observed set of tracks $\Sigma^- \rightarrow e^- p \pi^-$. There were two kinematic constraints, namely, the $\Lambda(p\pi^-)$ effective mass and the neutrino missing mass. The other four constraints were vertex constraints. Figure 6 shows a histogram of the χ^2 of the fit to the data compared to the χ^2 of the same fit performed on Monte Carlo generated events. The fitted momenta were then used in the determination of the form factors, as described below.

VI. $\Sigma^- \rightarrow \Lambda e^- \bar{\nu}$ RESULTS

To best use all the information available in each decay event, we can obtain a complete distribution function in the twelve-dimensional momentum space of the Λ , electron, neutrino, and proton. In this way, we take into account correlations in the momentum space in a relativistically correct way. Since the Λ decay is a good analyzer of the Λ polarization, Λ spin correlations will appear as proton momentum correlations in this space. The amplitude is obtained by summing the amplitude for the complete decay chain $\Sigma^- \rightarrow \Lambda e^- \bar{\nu}$, $\Lambda \rightarrow p \pi^-$ over the Λ spin. The square of the matrix element for the complete decay chain is given by Franzini *et al.*³ Figures 7 through 10 show experimental distributions of interest. The smooth curves show the Monte Carlo predicted distribu-

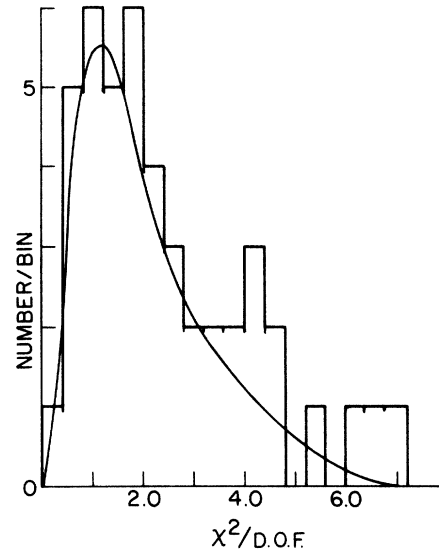


FIG. 6. χ^2 per degree of freedom of the 6-C fit to $\Sigma^- \rightarrow \Lambda e^- \bar{\nu}$. The smooth curve is the shape predicted by the Monte Carlo. In addition, there were eight events (not shown) with $\chi^2/\text{degree of freedom}$ greater than 7.2, while the Monte Carlo predicted there should be five such events.

tions as functions of $z = g_V/g_A$. These four distributions, for our level of statistics, contain essentially all the form-factor information and are essentially independent measurements. We performed separate maximum-likelihood fits for each

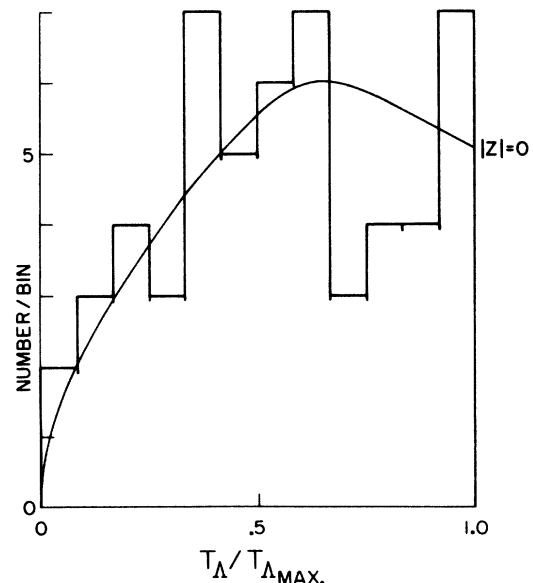
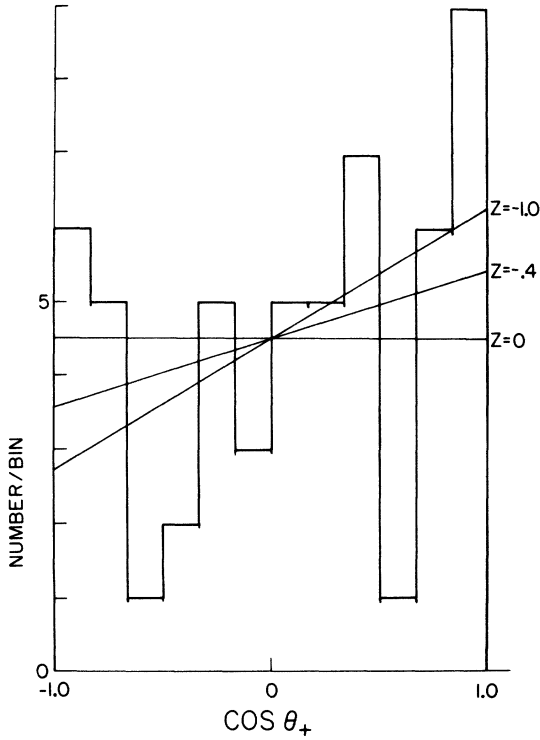


FIG. 7. Λ kinetic energy in Σ^- rest frame. Smooth curve is Monte Carlo prediction for $Z = g_V/g_A = 0$.

FIG. 8. $\cos\theta_+$ in Λ rest frame.

$$\cos\theta_+ = \frac{\vec{P}_p \cdot (\vec{P}_e + \vec{P}_\nu)}{|\vec{P}_p| |\vec{P}_e + \vec{P}_\nu|}$$

The expected distributions for several values of Z are shown.

distribution and combined the likelihood functions. The results of the maximum-likelihood fits are given in Table III.

The average detection efficiency for $\Sigma^- \rightarrow \Lambda e^- \bar{\nu}$ followed by $\Lambda \rightarrow p \pi^-$ was $3\frac{1}{2}\%$. Most of the loss was due to low momentum decay electrons hitting the spectrometer magnet. The electron spectrum (Fig. 10) is the only one of the four distributions which is significantly affected by the detection efficiency. Our result for g_V/g_A does not depend on the electron spectrum. Thus all systematic errors are small compared to the statistical error. The final result is²⁰

$$g_V/g_A = -0.25 \pm 0.35$$

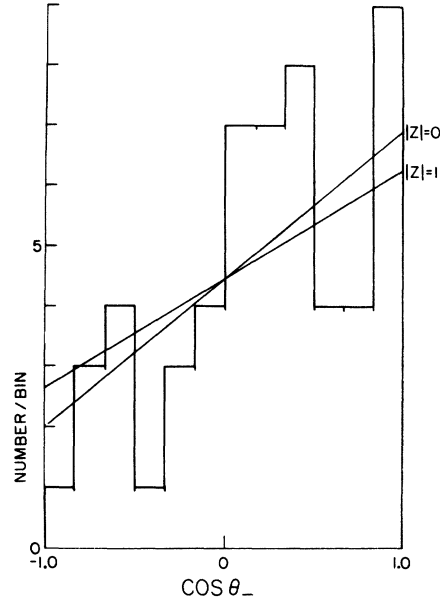
(assuming no weak magnetism)

or

$$g_V/g_A = -0.17 \pm 0.35$$

(assuming $g_{WM}/g_A = -1.9$ as predicted by CVC).

In addition, we can use the electron spectrum to determine g_{WM} . A maximum-likelihood fit for

FIG. 9. $\cos\theta_-$ in Λ rest frame.

$$\cos\theta_- = \frac{\vec{P}_p \cdot (\vec{P}_e - \vec{P}_\nu)}{|\vec{P}_p| |\vec{P}_e - \vec{P}_\nu|}$$

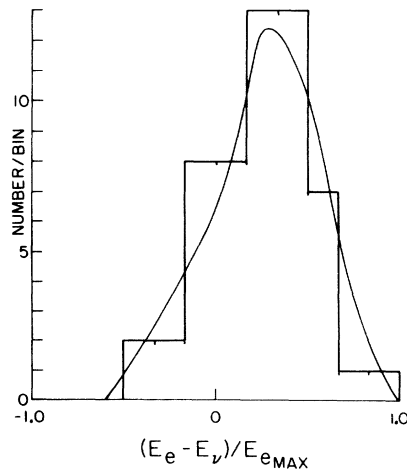
The expected distributions for several values of Z are shown.

g_{WM} , assuming $g_V = 0$, gives

$$g_{WM}/g_A = -3.5 \pm 4.5.$$

VII. $\Xi^- \rightarrow \Lambda e^- \bar{\nu}$ ANALYSIS AND RESULTS

$\Xi^- \rightarrow \Lambda e^- \bar{\nu}$ triggers were identical to $\Sigma^- \rightarrow \Lambda e^- \bar{\nu}$ triggers. $\Xi^- \rightarrow \Lambda e^- \bar{\nu}$ candidates were first required to meet the same criteria as $\Sigma^- \rightarrow \Lambda e^- \bar{\nu}$

FIG. 10. $(E_e - E_\nu)$ in Σ^- rest frame. The expected distribution is shown for $g_{WM} = 0$.

events, except for the final cut on the electron momentum.

Two additional cuts were imposed to eliminate $\Sigma^- \rightarrow \Lambda e^- \bar{\nu}$ events. First, the effective mass squared of the beam track, under the assumption of a $\Lambda e^- \bar{\nu}$ final state, was required to be greater than $1.60 \text{ GeV}^2/c^4$. Second, the kinetic energy of the Λ in the assumed Σ^- rest frame must be greater than 3.5 MeV. These two cuts eliminated virtually all $\Sigma^- \rightarrow \Lambda e^- \bar{\nu}$ from the sample, while eliminating only a negligible fraction of $\Xi^- \rightarrow \Lambda e^- \bar{\nu}$ events.

The separation of $\Xi^- \rightarrow \Lambda \pi^-$ background from $\Xi^- \rightarrow \Lambda e^- \bar{\nu}$ was more difficult, as the Q values for the two decays are similar. If an event met both of the following criteria, it was considered to be a $\Xi^- \rightarrow \Lambda \pi^-$ event and was, therefore, removed from the sample:

1. The effective mass squared of the beam track, reconstructed under the assumption of $\Xi^- \rightarrow \Lambda \pi^-$ decay, was between 1.67 and $1.80 \text{ GeV}^2/c^4$.
2. The discrepancy in total longitudinal momentum between the beam track and the three charged tracks in the final state was less than $1.0 \text{ GeV}/c$.

This final requirement eliminated most $\Xi^- \rightarrow \Lambda \pi^-$ contamination, but also eliminated 20% of the real $\Xi^- \rightarrow \Lambda e^- \bar{\nu}$ decays. The net detection efficiency was then 6%. A six-constraint fit was then made on the observed tracks $\Xi^- \rightarrow e^- p \pi^-$, just as was done for $\Sigma^- \rightarrow \Lambda e^- \bar{\nu}$ events.

The final sample consists of eleven events. The background levels expected in the sample are

TABLE III. Results of maximum-likelihood fits in $\Sigma^- \rightarrow \Lambda e^- \bar{\nu}$.

(a) Maximum-likelihood fits for g_V/g_A		
Method	$g_{WM}=0$	$g_{WM}=-1.9$
Λ spectrum	0.0 ± 0.7	0.0 ± 0.7
θ_+	-0.40 ± 0.45	-0.32 ± 0.45
θ_-	0.0 ± 0.85	$+0.1 \pm 0.85$
Combined	-0.25 ± 0.35	-0.17 ± 0.35
Previous world average ³	$+0.37 \pm 0.20$	$+0.45 \pm 0.20$
New world average	$+0.16 \pm 0.17$	$+0.24 \pm 0.17$
(b) Maximum-likelihood fit for g_{WM}/g_A from electron spectrum assuming $g_V=0$		
$g_{WM}/g_A = -3.5 \pm 4.5$		

$\Xi^- \rightarrow \Lambda \pi^-$ 3 or 4 events,
 $\Sigma^- \rightarrow \Lambda e^- \bar{\nu}$ no events.

Figure 11 is a Dalitz plot of the eleven events. The data are insufficient to make a meaningful determination of the form factors.

VIII. CABIBBO FIT

A new Cabibbo fit, incorporating the above measurements for $\Sigma^- \rightarrow ne^- \bar{\nu}$ and $\Sigma^- \rightarrow \Lambda e^- \bar{\nu}$ into the

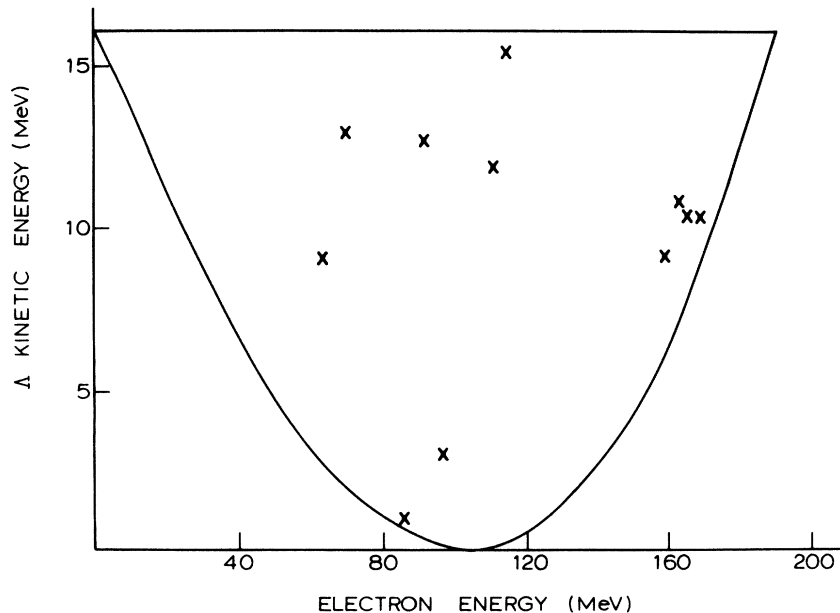


FIG. 11. Dalitz plot for $\Xi^- \rightarrow \Lambda e^- \bar{\nu}$ decay.

world average, was performed in the identical manner as that of the one-angle fit of Ebenhoh *et al.*²¹ The new world-average values used in this fit were

$$\begin{aligned}\Sigma^- \rightarrow ne^{-}\bar{\nu}, \quad g_A/g_V = 0.413 \pm 0.033 \text{ (sign assumed),} \\ \Sigma^- \rightarrow \Lambda e^{-}\bar{\nu}, \quad g_V/g_A = +0.24 \pm 0.17.\end{aligned}$$

These are weighted averages of our results with the previous results in the 1974 Review of Particle Properties.²² All other form-factor ratios, branching ratios, and lifetimes used were those in the 1974 Review of Particle Properties. It should be pointed out that a g_V/g_A measurement in $\Sigma^- \rightarrow \Lambda e^{-}\bar{\nu}$ does not affect the fitted values of θ , f , or d , since for this decay $g_V/g_A = 0$ by CVC, regardless of the values of the Cabibbo parameters. Such a measurement does, however, affect the goodness of fit. The errors are not scaled to allow for uncertainties in the slopes of the form factors.

The assumptions used were:

(a) The induced scalar and the pseudotensor contributions were assumed to be absent, the weak magnetism form factor was determined from CVC using a correction factor for the octet mass splitting, the pseudoscalar form factor taken from the Goldberger-Treiman relation. Our results are not sensitive to these assumptions.

(b) The q^2 dependence of all form factors has been parametrized as $f_i(q^2) = f_i(0)(1 + \lambda_i q^2)$. The choice of the slopes λ_i is of some influence on the fit. The slopes of the vector and weak-magnetism form factors are predicted by CVC.¹⁶ The slope of the axial-vector form factor is assumed to be one-half that of the vector form factor.¹⁶ Ebenhoh *et al.*²¹ found that varying the slopes within reasonable limits caused the parameters to vary within about 1 standard deviation, and have scaled their quoted errors to account for this. We have neither varied the slopes nor scaled our quoted errors.

The results of the fit are

$$\begin{aligned}\theta &= 0.232 \pm 0.003, \\ f &= 0.436 \pm 0.010, \\ d &= 0.812 \pm 0.011,\end{aligned}$$

with a χ^2 of 8.53 for 8 degrees of freedom. The errors are correlated; the full error matrix is

	θ	f	d
θ	1.068×10^{-5}	-8.315×10^{-6}	1.434×10^{-5}
f	-8.315×10^{-6}	9.508×10^{-5}	-6.669×10^{-5}
d	1.434×10^{-5}	-6.669×10^{-5}	1.150×10^{-4}

IX. CONCLUSIONS

The form-factor result for $\Sigma^- \rightarrow ne^{-}\bar{\nu}$ from this experiment is consistent with the Cabibbo theory and significantly improves the accuracy to which the parameters are determined. The study of hyperon leptonic decays has reached the point where (i) expected deviations from the simple Cabibbo theory due to SU(3) breaking effects, (ii) uncertainties in the q^2 dependence of form factors, and (iii) the possible existence of second-class currents cause larger uncertainties in theoretical predictions of form factors and decay rates than do the experimental errors in the Cabibbo parameters themselves. The Cabibbo theory has thus been as successful as could be expected. It should be pointed out, however, that the sign of g_A/g_V in $\Sigma^- \rightarrow ne^{-}\bar{\nu}$ decay is still experimentally unknown, as is g_A/g_V itself for all Ξ^- and Ξ^0 leptonic decays and all muonic hyperon decays.

The form-factor results for $\Sigma^- \rightarrow \Lambda e^{-}\bar{\nu}$ are consistent with the CVC prediction $g_V = 0$. The present total world sample of $\Sigma^- \rightarrow \Lambda e^{-}\bar{\nu}$ is only about 200 events.

ACKNOWLEDGMENTS

We wish to thank our engineering staff, Andy Disco, Satish Dhawan, Cordon Kerns, Stan Ladzinski, Blaise Lombardi, and Irving Winters, and our technicians Alan Wandersee, Jon Blomquist, and Ed Steigmeyer for their help in the design and setup of the apparatus. We also thank the AGS staff, in particular, David Berley, Eugene Halek, and Gerry Tanguay for providing the technical support needed for the success of this experiment. We also thank the University of Pittsburgh group for use of the proton calorimeter.

APPENDIX I. MONTE CARLO PROGRAM

The expected physical distributions used in the various maximum-likelihood fits to the form factors were calculated by the Monte Carlo method.

Let g represent the collective values of all the form factors. Let $P_i^{(k)}(g)$ be the probability that one theoretically generated event chosen at random will fall in bin i of distribution k , without taking into account experimental errors or detection efficiency. $P_i^{(k)}(g)$ can easily be determined for any value of the form factors, since it depends only on the decay matrix element and is completely independent of experimental details. Events were generated with a uniform distribution on the Dalitz plot. In the case of $\Lambda \rightarrow p\pi^-$, the decay was generated isotropically in the Λ rest frame. The distribution $P_i^{(k)}(g)$ was then calculated simply by

weighting each event by the square of the matrix element.

Let $F_{ji}^{(k)}$ be the probability that one event chosen at random, actually belonging in bin i of the distribution, will be experimentally found in bin j of that distribution. $F_{ji}^{(k)}$ must be normalized so that $\sum_j F_{ji}^{(k)} = E_i^{(k)}$, where $E_i^{(k)}$ is the experimental detection efficiency for events occurring in bin i . If the bins are sufficiently small, such that events within a single bin are distributed uniformly, $F_{ji}^{(k)}$ is independent of the form factors and thus need be calculated only once. It essentially contains the entire effect of experimental error and detection efficiency. $F_{ji}^{(k)}$ is calculated by Monte Carlo techniques, using experimentally determined resolution functions. The Σ^- and Ξ^- production spectra were chosen according to our own previous measurements. Decays were chosen to be uniformly distributed on the Dalitz plot and spatially isotropic. Included in the calculation were the geometry of the apparatus and the magnetic field, including the fringe field and verticle focusing. Experimentally determined effects of spark-chamber efficiency and resolution and neutron-detector resolution were also included.

Once the simulated events were constructed in the laboratory, the same programs used in the analysis of the true events were used to reconstruct the simulated events with identical cuts. After the events are reconstructed, the reconstructed events are compared to the originally generated events to calculate $F_{ji}^{(k)}$ for each relevant distribution.

The number of events expected experimentally in bin j of distribution k is simply

$$N_j^{(k)}(g) = Q \sum_i F_{ji}^{(k)} P_i^{(k)}(g), \quad (14)$$

where Q is a normalizing factor such that $\sum_j N_j^{(k)}$ equals the total number of events in the sample. The N_j are used in the final likelihood fit.

APPENDIX II. MUON BACKGROUND

The measured singles rate in the 25-cm \times 25-cm hole veto (V_H) was about 2×10^6 counts/pulse. Thus, for every pulse, there were more than two-million charged particles emerging from the shielding around the hyperon channel. These par-

ticles were positive and negative muons which formed a halo around the beam. The muons came from the decays in flight of pions produced in the C-target (a 4-cm copper target located far upstream in the incident proton beam), the hyperon-production target, and elsewhere. Muons bent out of the incident proton beam or the hyperon beam channel by magnets were bent back toward the proton beam by the return field of the magnets. Many muons thus remained trapped in a region surrounding the hyperon beam.

The total singles rate in the S counters, an area of 1.25 m², was typically 1.5×10^6 counts/sec, the great majority of them muons. Most muons emerging from the shielding were over the Čerenkov threshold of 6.2 GeV/ c . The trigger logic required a Čerenkov count within a 10-nsec interval. We thus expect an accidental Čerenkov count once in 67 nonleptonic events, consistent with the 1 in 80 actually observed.

APPENDIX III. BRANCHING RATIOS

Our leptonic branching-ratio measurements suffer from systematic normalization uncertainties of about 20%, the greatest of which are the absolute efficiencies of the Čerenkov counter and the time-of-flight logic. Nevertheless, we can use known branching ratios as consistency checks. Our measured $(\Sigma^- \rightarrow ne^- \bar{\nu})/(\Sigma^- \rightarrow n\pi^-)$ branching ratios are

$$\text{for 6-kG m data } (0.98 \pm 0.03) \times 10^{-3},$$

$$\text{for 13-kG m data } (0.88 \pm 0.03) \times 10^{-3},$$

where the quoted errors are statistical only. The accepted value is $(1.08 \pm 0.04) \times 10^{-3}$. Given our systematic normalization uncertainties, we consider these results to be consistent with previous experiments.

The accepted $(\Sigma^- \rightarrow \Lambda e^- \bar{\nu})/(\Sigma^- \rightarrow ne^- \bar{\nu})$ branching ratio is $\frac{1}{18}$. Our detection efficiency for $\Sigma^- \rightarrow \Lambda e^- \bar{\nu}$ is $\frac{1}{3}$ that for $\Sigma^- \rightarrow ne^- \bar{\nu}$. We therefore expect one $\Sigma^- \rightarrow \Lambda e^- \bar{\nu}$ event for every 54 $\Sigma^- \rightarrow ne^- \bar{\nu}$ events, or 65 $\Sigma^- \rightarrow \Lambda e^- \bar{\nu}$ events. We saw 55 such events.

From our sample of good decays and the known $(\Xi^- \rightarrow \Lambda e^- \bar{\nu})/(\Xi^- \rightarrow \Lambda \pi^-)$ branching ratio, we expect about 15 $\Xi^- \rightarrow \Lambda e^- \bar{\nu}$ events. We saw 11 such events. We consider this to be reasonable agreement between our expectations and measurements.

*Present address: SLAC, Stanford, California

†Present address: Université de Genève, Geneva, Switzerland.

‡Present address: CERN, Geneva, Switzerland.

§Research supported by the U. S. Atomic Energy Commission under Contract No. AT(11-1).

¶Operated by Universities Research Association, Inc. under contract with the U. S. Atomic Energy Com-

mission.

† Work supported in part by the U. S. Atomic Energy Commission.

- ¹D. R. Harrington, Phys. Rev. 120, 1482 (1960). The expression $(1 + \gamma^5)$ has been replaced by $(1 - \gamma^5)$. This sign convention is consistent with that of Ref. 22.
- ²No. Cabibbo, Phys. Rev. Lett. 10, 531 (1963).
- ³P. Franzini *et al.*, Phys. Rev. D 6, 2417 (1972).
- ⁴A. P. Colleraine *et al.*, Phys. Rev. Lett. 23, 199 (1969).
- ⁵F. Eisele *et al.*, Z. Phys. 223, 487 (1969).
- ⁶C. Baltay *et al.*, Phys. Rev. D 5, 1569 (1972).
- ⁷J. Lindquist *et al.*, Phys. Rev. Lett. 27, 612 (1971); K. H. Althoff *et al.*, Phys. Lett. 37B, 535 (1971); 43B, 237 (1973).
- ⁸R. Feynman and M. Gell-Mann, Phys. Rev. 109, 193 (1958); N. Cabibbo and R. Gatto, Nuovo Cimento 15, 159 (1960).
- ⁹S. Weinberg, Phys. Rev. 112, 1375 (1958); P. Hertel, Z. Phys. 202, 383 (1967).
- ¹⁰V. Hungerbühler *et al.*, Nucl. Instrum. Methods 115, 221 (1974).
- ¹¹V. Hungerbühler *et al.*, Phys. Rev. D 12, 1203 (1975).
- ¹²W. J. Willis *et al.*, Nucl. Instrum. Methods 91, 33 (1971).
- ¹³M. Atac *et al.*, Nucl. Instrum. Methods 106, 263 (1973).
- ¹⁴W. Tanenbaum, Nucl. Instrum. Methods 106, 269 (1973).
- ¹⁵The $\Sigma^- \rightarrow ne^- \bar{\nu}$ experiment is discussed in detail in W. Tanenbaum, Ph.D. thesis, Yale University, 1974 (unpublished).
- ¹⁶I. Bender, V. Linke, and M. Rothe, Z. Phys. 221, 190 (1968).
- ¹⁷For hyperon leptonic decays the momentum transfer is timelike ($q^2 > 0$). Hence, CVC predicts that the vector form factor increases with increasing q^2 .
- ¹⁸See, for example, R. E. Marshak, Riazuddin, and C. P. Ryan, *Theory of Weak Interactions in Particle Physics* (Wiley-Interscience, New York, 1969), pp. 323-326.
- ¹⁹This value of λ_A is expected if the q^2 dependence of the axial-vector form factor is determined by the A_1 meson pole.
- ²⁰In our conventions, g_A/g_V is negative in neutron β decay and g_{WM} is made dimensionless by division by the Σ mass.
- ²¹H. Ebenhoeh *et al.*, Z. Phys. 241, 473 (1971); F. Eisele *et al.*, *ibid.* 225, 383 (1969).
- ²²Particle Data Group, Phys. Lett. 50B, 1 (1974).